ISSN: 0067-2904

Mathematical Modelling for Peristaltic Flow of Sutterby Fluid Through Tube under the Effect of Endoscope

Neeran Ammar, Hayat A. Ali*
Department of Applied Science, University of Technology, Baghdad, Iraq

Received: 26/2/2022 Accepted: 19/8/2022 Published: 30/5/2023

Abstract

In this work, the mathematical modelling of peristaltic transport for incompressible Sutterby fluid through the cavity between coaxial tubes where the inner tube is fixed and the outer tube has sinusoidal rhythmic fluctuations along the channel's walls is presented. Under the assumption of long wavelength and the low Reynolds number, the governing equations (motion, temperature, and concentration) are illustrated in cylindrical coordinates. The analytical solution for the temperature and concentration of the fluid flow is obtained using Mathematica 11.3, whereas the perturbation technique is employed to find the closed form of the velocity profile. The variation of the axial velocity, stream function, temperature, concentration, and heat transfer are graphically discussed under the impact of interesting involved parameters.

Keywords: Peristaltic Flow, Sutterby Fluid, Endoscope.

النمذجة الرياضية للتدفق التمعجي لمائع سوتيربي عبر أنبوب تحت تأثير المنظار الداخلي

نيران عمار، حياة عادل علي*
قسم العلوم التطبيقية, الجامعة التكنولوجية, بغداد, العراق

الخلاصة

في هذا العمل، تم تقديم النمذجة الرياضية للنقل التمعجي لسائل سوتيربي الغير قابل للانضغاط خلال الفجوة بين الأنابيب المحورية بحيث يتم تثبيت الأنبوب الداخلي ويكون للأنبوب الخارجي تقلبات إيقاعية جيبية على طول جدران القناة. في ظل افتراض الطول الموجي الطويل وعدد رينولدز المنخفض، تم توضيح المعادلات الحاكمة (الحركة ودرجة الحرارة والتركيز) في إحداثيات أسطوانية. تم الحصول على الحلول التحليلية لدرجة الحرارة وتركيز التدفق المائع باستخدام Mathematica 11.3، بينما تم استخدام تقنية الاضطراب للعثور على الشكل المغلق لملف السرعة. تمت مناقشة اختلاف السرعة المحورية ووظيفة التدفق ودرجة الحرارة والتركيز ونقل الحرارة بيانياً تحت تأثير المعلمات المعنية المثيرة للاهتمام.

1. Introduction

The mechanism of peristalsis has gathered essential attention in our life due to its rapid increase, mostly encountered in engineering, scientific and medical aspects. Peristalsis assists in flowing through the channel because of the successive contraction and relaxation emerging

*Email: Hayat.A.Ali@uotechnology.edu.iq

along the walls of the channel [1].This phenomenon facilitates the transport of many fluids in touch with the physiological organs, like the kidney, bladder, lymphatic vessels; the oesophagus tube; the gastrointestinal tract, etc. The first theoretical study of peristalsis was given by Latham [2].While Shapiro et al. [3] and Jaffrin et al. [4] developed this study to include some practical applications. Recently, many investigations analyzed peristaltic transport, some listed in [5] [6] [7] [8].

Functional relations or nonlinearity shear stress. Also, the variant in fluid viscosity recognized or identified the non-Newtonian fluid. Many industrial processes for non-Newtonian fluids appear in formulations of pharmaceuticals, foodstuffs, cosmetics and toiletries, paints, etc. Considerable studies depend on non-Newtonian fluids. The peristaltic transport of Newtonian and non-Newtonian fluids concern of great interest to many researchers [9] [10] [11] [12] [13] [14].An extensive exploration discussed the peristalsis mechanism for numerous non- Newtonian fluids [15].The first progress in the aforementioned consideration is illustrated by Raju and Devanathan [16]. An interesting non- Newtonian fluid modelled high polymer aqueous solutions called Sutterby fluid [17]. Khan et al. [18]. investigated the effect of homogeneous-heterogeneous reactions on the Sutterby fluid flow through a rotating disk. Hayat et al. [19]. investigated the Sutterby fluid radiative flow caused by a revolving disk with a chemical reaction and a changing thickness. While, Rao et al. [20] studied the flow, heat, and mass transfer of a Sutterby fluid bio fluid towards a stretching sheet saturated with a porous medium while taking viscous dissipation into account. Whereas, Mabood et al. [21] used the Stefan blowing and non-Fourier/Fick models to study the Sutterby material flow caused by a rotating stretchable disk. In 2017 Hayat et al. [22] examined the peristaltic flow of Sutterby fluid in a planar symmetric channel by employing the modified Darcy's law for the porous medium effect.

The endoscope is an optical illumination system used to get an intense look into the body. An endoscope is a surgical device comprised of a thin, long, and flexible (or rigid) tube that involves a light and video camera at one end to show organs such as the throat or oesophagus, or any part of the human body needed to be looked for example the cystoscope (bladder), gastrointestinal endoscopes, arthroscope (joint), and bronchoscope (bronchi). For a medical diagnosis, an endoscope's impact on peristaltic motion is very significant as well as it has many clinical applications. It is a sensitive method for recognizing the causes of any complications in the peristaltic pumping of the fluid in human organs [1]. Ramesh and Devakar [23] studied the biomedicine application impacts of an endoscope and heat transfer on the peristaltic transport of a couple of stress fluids. Whereas Hayat et al. [24] numerically solved the peristaltic activity of MHD flow of Williamson nanofluid saturating porous space taking into account that the inner tube is an endoscope.

There is no search available for the link between the endoscope and Sutterby fluid. In the current paper, we have focused on the influence of the endoscope on the Peristaltic Flow of Sutterby fluid. The flow equations of Sutterby fluid are modelled depending on the conservation of mass, movement, temperature, and concentration equations in the cylindrical coordinate system. A long wave number and low Reynolds number are taken into consideration to simplify the problem. The perturbation technique is used to solve the motion equations and find the last shape of the stream function. Finally, the effects of various parameters on velocity profile, temperature profile, Concentration profile, and heat transfer coefficients are graphically discussed.

2. Mathematical Formulation

The peristaltic transport of a non-Newtonian Sutterby model through a uniform channel is considered. The inner and outer concentric tubes formed the endoscope and peristaltic tubes, respectively. The cylindrical coordinate system is chosen and mannered in which $\tilde{Z}$ coordinate is considered across the centerline of the tube and $\tilde{R}$ is across the radial tendency. The temperatures and the fluid concentration of the inner and outer tubes are $T_0, C_0,\ T_1,$ and C_1 respectively see Figure 1.

The mathematical model of the tube wall is defined as:

$$\tilde{R}_1 = a_1 \tag{1}$$

$$\tilde{R}_2 = a_2 + b\ Cos\left(\frac{2\pi}{\lambda}(\tilde{Z} - c\tilde{t})\right) \tag{2}$$

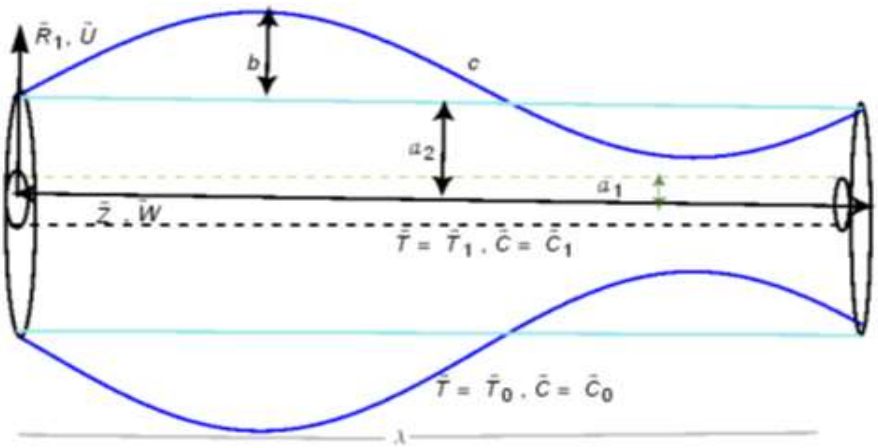

Figure 1: Geometry of channel

where a_1 is the inner tube radius, a_2 is the average radius of the outer tube at the inlet, b is the amplitude of the wave, λ is the wavelength, c represents the velocity of the peristaltic wave and $\tilde{t}$ is the time. Taking the above flow properties into account, the following equations govern the fluid flow in the laboratory frame of reference.
The continuity equation has the form:

$$\frac{\partial \tilde{U}}{\partial \tilde{R}} + \frac{\tilde{U}}{\tilde{R}} + \frac{\partial \tilde{W}}{\partial \tilde{Z}} = 0\ , \tag{3}$$

and the momentum equations are

$$\rho\left(\frac{\partial \tilde{U}}{\partial \tilde{t}} + \tilde{U}\frac{\partial \tilde{U}}{\partial \tilde{R}} + \tilde{W}\frac{\partial \tilde{U}}{\partial \tilde{Z}}\right) = -\frac{\partial \tilde{P}}{\partial \tilde{R}} + \frac{1}{\tilde{R}}\frac{\partial}{\partial \tilde{R}}(\tilde{R}\tilde{S}_{\tilde{R}\tilde{R}}) + \frac{\partial}{\partial \tilde{Z}}(\tilde{S}_{\tilde{R}\tilde{Z}})\ - \frac{\tilde{S}_{\tilde{\theta}\tilde{\theta}}}{\tilde{R}}, \tag{4}$$

$$\rho\left(\frac{\partial \tilde{W}}{\partial \tilde{t}} + \tilde{U}\frac{\partial \tilde{W}}{\partial \tilde{R}} + \tilde{W}\frac{\partial \tilde{W}}{\partial \tilde{Z}}\right) = -\frac{\partial \tilde{P}}{\partial \tilde{Z}} + \frac{1}{\tilde{R}}\frac{\partial}{\partial \tilde{R}}\left(\tilde{R}\tilde{S}_{\tilde{R}\tilde{Z}}\right) + \frac{\partial}{\partial \tilde{Z}}\left(\tilde{S}_{\tilde{Z}\tilde{Z}}\right). \tag{5}$$

Also, the energy equation has the form

$$\rho C_p\left(\frac{\partial \tilde{T}}{\partial \tilde{t}} + \tilde{U}\frac{\partial \tilde{T}}{\partial \tilde{R}} + \tilde{W}\frac{\partial \tilde{T}}{\partial \tilde{Z}}\right) = K\left(\frac{\partial^2 \tilde{T}}{\partial \tilde{R}^2} + \frac{\partial^2 \tilde{T}}{\partial \tilde{Z}^2} + \frac{1}{\tilde{R}}\frac{\partial \tilde{T}}{\partial \tilde{R}}\right) + \frac{D_m K_T}{C_s}\left(\frac{\partial^2 \tilde{C}}{\partial \tilde{R}^2} + \frac{\partial^2 \tilde{C}}{\partial \tilde{Z}^2} + \frac{1}{\tilde{R}}\frac{\partial \tilde{C}}{\partial \tilde{R}}\right) -$$
$$\frac{1}{\tilde{R}}\frac{\partial}{\partial \tilde{R}}\left(\tilde{R}\ q_{\tilde{R}}\right) + Q \tag{6}$$

where the Roseland approximation for radiation $q_{\tilde{R}}$ is given by [25]

$$q_{\tilde{R}} = \frac{-4\sigma^*}{3k^*}\frac{\partial T^4}{\partial \tilde{R}}, \tag{7}$$

σ^* and k^* are the Stefan-Boltzmann constant and Rosseland absorption coefficient approximation, respectively. Expanded T^4 by using the Taylor series. Thus, by neglecting the higher-order terms as

$$T^4 = 4T_0^3 T - 3T_0^4. \tag{8}$$

Hence, Eq. (6) replaced into

$$\rho C_p \left(\frac{\partial \tilde{T}}{\partial \tilde{t}} + \widetilde{U}\frac{\partial \tilde{T}}{\partial \tilde{R}} + \widetilde{W}\frac{\partial \tilde{T}}{\partial \tilde{Z}}\right) = K\left(\frac{\partial^2 \tilde{T}}{\partial \tilde{R}^2} + \frac{\partial^2 \tilde{T}}{\partial \tilde{Z}^2} + \frac{1}{\tilde{R}}\frac{\partial \tilde{T}}{\partial \tilde{R}}\right) + \frac{D_m K_T}{C_s}\left(\frac{\partial^2 \tilde{C}}{\partial \tilde{R}^2} + \frac{\partial^2 \tilde{C}}{\partial \tilde{Z}^2} + \frac{1}{\tilde{R}}\frac{\partial \tilde{C}}{\partial \tilde{R}}\right) - \frac{1}{\tilde{R}}\frac{\partial}{\partial \tilde{R}}\left(\tilde{R}\frac{-16T_0^3\sigma^*}{3k^*}\frac{\partial T}{\partial \tilde{R}}\right) + Q \tag{9}$$

The concentration equation is

$$\left(\frac{\partial \tilde{C}}{\partial \tilde{t}} + \widetilde{U}\frac{\partial \tilde{C}}{\partial \tilde{R}} + \widetilde{W}\frac{\partial \tilde{C}}{\partial \tilde{Z}}\right) = D_m\left(\frac{\partial^2}{\partial \tilde{R}^2} + \frac{1}{\tilde{R}}\frac{\partial}{\partial \tilde{R}} + \frac{\partial^2}{\partial \tilde{Z}^2}\right)\tilde{C} + \frac{D_m K_T}{T_m}\left(\frac{\partial^2}{\partial \tilde{R}^2} + \frac{1}{\tilde{R}}\frac{\partial}{\partial \tilde{R}} + \frac{\partial^2}{\partial \tilde{Z}^2}\right)\tilde{T} \tag{10}$$

Where $\widetilde{U}, \widetilde{W}, \rho, \tilde{T}, \tilde{P}, C_p, K, \tilde{C}, D_m, K_T, C_s, Q$and T_m are the fixed frame components of velocity, the fluid density, the temperature field, the pressure, the constant pressure specific heat, the electrical conductivity, the concentration field, Brownian diffusion coefficient, ratio of thermal diffusion, concentration susceptibility, generation/absorption parameter and mean temperature, respectively. The $\tilde{S}_{\tilde{R}\tilde{R}}, \tilde{S}_{\tilde{R}\tilde{Z}}$ and $\tilde{S}_{\tilde{\theta}\tilde{\theta}}$ are the extra stress tensor components.
where the expression of extra stress tensor for a non-Newtonian Sutterby fluid is given by the relation [18].

$$\tilde{S}_{ij} = \frac{\mu}{2}\left(\frac{sinh^{-1}\beta^*\dot{\gamma}}{\beta^*\dot{\gamma}}\right)^m \widetilde{A} \tag{11}$$

$$\widetilde{A} = grad(V) + \left(grad(V)\right)^T \tag{12}$$

$$\dot{\gamma} = \sqrt{\frac{\Pi}{2}}, \ where\ \Pi = tr\left[grad(V) + \left(grad(V)\right)^T\right]^2 \tag{13}$$

$\tilde{S}_{ij}$ is the extra stress tensor, β^* and m are the Sutterby fluid constants, μ is the dynamic viscosity coefficient, $\widetilde{A}$ is the first Rivilin Ericksen tensor, $\dot{\gamma}$ is the shear rate and dots over the quantities indicate differentiation concerning time, and Π is the second invariant strain tensor.
The dimensional mathematical form for the problem boundary conditions are

$$\widetilde{W} = 0, \widetilde{U} = 0, \ at\ \ \tilde{R}_1, \tilde{R}_2, \tag{14}$$

$$\begin{bmatrix} \tilde{T} = \tilde{T}_1, \tilde{C} = \tilde{C}_1\ at\ \tilde{R}_1 \\ \tilde{T} = \tilde{T}_0, \tilde{C} = \tilde{C}_0\ at\ \tilde{R}_2 \end{bmatrix} \tag{15}$$

Utilizing the following mathematical equations that relate to the fixed $(\tilde{R}, \tilde{Z})$and moving frames, the unsteady flow between the two tubes becomes steady in a wave frame $(\tilde{r}, \tilde{z})$ moving with the same speed as a wave in the $\tilde{Z}$ direction.

$$\tilde{r} = \tilde{R}\ , \tilde{z} = \tilde{Z} - c\tilde{t}\ ,\ \tilde{u} = \widetilde{U}\ \ ,\ \tilde{w} = \widetilde{W} - c, \tilde{p} = \tilde{P}\ \ \ , \tag{16}$$

Introducing the following dimensionless transformations for facilitating the governing equations of the motion as follows [24] [25]:

$$r=\frac{\tilde{r}}{a_2}, z=\frac{\tilde{z}}{\lambda}, u=\frac{\tilde{u}}{c\delta}, w=\frac{\tilde{w}}{c}, \theta=\frac{\tilde{T}-T_0}{T_1-T_0}, \tilde{S}_{ij}=\frac{a_2}{\mu c}\tilde{S}_{ij}, Pr=\frac{\mu c\rho}{K}, Re=\frac{\rho c a_2}{\mu},$$
$$B=\frac{{a_2}^2 Q}{k(T_1-T_0)}, Gr=\frac{\rho g\alpha(T_1-T_0){a_2}^2}{\mu c}, r_1=\frac{\tilde{r}_1}{a_2}, Rn=\frac{16\,{T_\infty}^3\sigma^*}{3\,k^*K}, Sc=\frac{\upsilon}{D_m}, Sr=\frac{D_m K_T T_0}{\upsilon T_m C_0}, Du=$$
$$\frac{D_m K_T C_0}{\mu C_P C_S T_0}, Pr=\frac{\mu C_P}{K}, \eta=\frac{\tilde{C}-C_0}{C_1-C_0}, \epsilon=\frac{b}{a_2}, \alpha=\frac{mc^2\beta^{*2}}{{a_2}^2} \quad (17)$$

Compensate Eq. (17) into equations (1)-(15), this leads to simplifying the equations into the following form

$$\frac{\partial u}{\partial r}+\frac{u}{r}+\frac{\partial w}{\partial z}=0 \quad (18)$$

Adopting the assumptions of long-wavelength approximation and small Reynold's number that means dropping terms of order δ and the higher Eqs. (15) -(18) are simplified to

$$Re\,\delta^3\left(u\frac{\partial u}{\partial r}+(w+1)\frac{\partial u}{\partial z}\right)=-\frac{\partial P}{\partial r}+\delta\frac{1}{r}\frac{\partial}{\partial r}(rS_{rr})+\delta^2\frac{\partial}{\partial z}(S_{rz})-\delta\frac{S_{\theta\theta}}{r}, \quad (19)$$
$$Re\,\delta\left(u\frac{\partial w}{\partial r}+(w+1)\frac{\partial w}{\partial z}\right)=-\frac{\partial P}{\partial z}+\frac{1}{r}\frac{\partial}{\partial r}(rS_{rz})+\delta\frac{\partial}{\partial z}(S_{zz}), \quad (20)$$
$$Re\,Pr\delta\left(u\frac{\partial\theta}{\partial r}+(w+1)\frac{\partial\theta}{\partial z}\right)=\left(\frac{\partial^2\theta}{\partial r^2}+\delta^2\frac{\partial^2\theta}{\partial z^2}+\frac{1}{r}\frac{\partial\theta}{\partial r}\right)+DuPr\left(\frac{\partial^2\eta}{\partial r^2}+\delta^2\frac{\partial^2\eta}{\partial z^2}+\frac{1}{r}\frac{\partial\eta}{\partial r}\right)+$$
$$Rn\left(\frac{1}{r}\frac{\partial\theta}{\partial r}+\frac{\partial^2\theta}{\partial r^2}\right)+B, \quad (21)$$
$$Re\delta\left(u\frac{\partial\eta}{\partial r}+(w+1)\frac{\partial\eta}{\partial z}\right)=\left(\frac{\partial^2\eta}{\partial r^2}+\frac{1}{r}\frac{\partial\eta}{\partial r}+\delta^2\frac{\partial^2\eta}{\partial z^2}\right)+ScSr\left(\frac{\partial^2\theta}{\partial r^2}+\frac{1}{r}\frac{\partial\theta}{\partial r}+\delta^2\frac{\partial^2\theta}{\partial z^2}\right), \quad (22)$$

where Re is the Reynolds number, u and w are the radials and axial velocity, respectively . While δ is the wave number, θ is temperature, η is concentration,Pr is the Prandtl number, Du is the Dufour number, Rn is the radiation parameter, Sc is the Schmidt number and Sr is the Soret number. Adopting the assumption of long-wavelength $\delta \ll 1$ and low Reynolds number Eqs. (19)-(22) reduced to the forms

$$\frac{\partial P}{\partial r}=0, \quad (23)$$
$$\frac{\partial P}{\partial z}=\frac{1}{r}\frac{\partial}{\partial r}(rS_{rz}), \quad (24)$$
$$(1+Rn)\left(\frac{\partial^2\theta}{\partial r^2}+\frac{1}{r}\frac{\partial\theta}{\partial r}\right)+DuPr\left(\frac{\partial^2\eta}{\partial r^2}+\frac{1}{r}\frac{\partial\eta}{\partial r}\right)+B=0, \quad (25)$$
$$\frac{\partial^2\eta}{\partial r^2}+\frac{1}{r}\frac{\partial\eta}{\partial r}+SrSc\left(\frac{\partial^2\theta}{\partial r^2}+\frac{1}{r}\frac{\partial\theta}{\partial r}\right)=0, \quad (26)$$

The previous equations are combined with the dimensionless boundary conditions:

$$w=-1, u=0, \quad at \quad r_1=\beta, \; and \quad r_2=1+\epsilon\cos(2\pi z) \quad (27)$$
$$\begin{bmatrix} \theta=1, \eta=1 & at \quad r_1=\beta \\ \theta=0, \eta=0 & at \quad r_2=1+\epsilon\cos(2\pi z) \end{bmatrix} \quad (28)$$

where

$$s_{zr}=s_{rz}=\frac{1}{r}w_r-\frac{\alpha}{12}{w_r}^3, \text{and } s_{rr}=s_{zz}=0 \quad (29)$$

Equation (23) reveals that the pressure field independent from r, i.e. p is a function of z only.

3. Solution of the problem

3.1. Solution of Temperature and Concentration Equations

The system of equations (25), and (26) with the associated boundary conditions listed in equation (28) are solved with the help of MATHEMATIC program. The explicit expressions for the solutions of θ and η ,respectively, are given as follows:

$$\theta(r) = (4Log(r) + Br_1{}^2Log(r) - B\,r_2{}^2Log(r) + 4RnLog(r) - 4DuPrScSrLog(r) - Br^2Log(r_1) + Br_2{}^2Log(r_1) - 4Log(r_2) + Br^2Log(r_2) - Br_1{}^2Log(r_2) - 4RnLog(r_2) + 4DuPrScSrLog(r_2))/(4(1 + Rn - DuPrScSr)(Log(r_1) - Log(r_2))) \quad (30)$$

$$\eta(r) = -((-4Log(r) - 4RnLog(r) + 4DuPrScSrLog(r) + Br_1{}^2ScSrLog(r) - Br_2{}^2ScSrLog(r) - Br^2ScSrLog(r_1) + Br_2{}^2ScSrLog(r_1) + 4Log(r_2) + 4RnLog(r_2) - 4DuPrScSrLog(r_2) + Br^2ScSrLog(r_2) - Br_1{}^2ScSrLog(r_2))/(4(1 + Rn - DuPrScSr)(Log(r_1) - Log(r_2)))) \quad (31)$$

3.2. Solution of motion Equation

It is difficult to obtain the exact solution of the nonlinear motion equation (24), we implement the perturbation method for small values of the Sutterby parameter α in the following form:

$$w = w_0 + \alpha w_1 + O(\alpha^2) \quad (32)$$

Substitute Eq. (32) into Eq. (24), and arranging in terms of the similar powers of α, we have the following systems:

zeroth-order system of α^0 as

$$\frac{dp}{dz} = \frac{\partial^2 w_0}{\partial r^2} + 0.5\frac{\partial w_0}{\partial r} \quad (33)$$

associated with the boundary conditions

$$w_0 = -1 \quad at \quad r_1 = \beta, \; and \quad r_2 = 1 + \epsilon\, cos(2\pi z) \quad (34)$$

and first-order system of α^1 as

$$\frac{\partial^2 w_1}{\partial r^2} + 0.5\frac{\partial w_1}{\partial r} - \frac{1}{12\,r}\left(\frac{\partial w_0}{\partial r}\right)^3 - \frac{1}{4}\left(\frac{\partial w_0}{\partial r}\right)^2\frac{\partial^2 w_0}{\partial r^2} = 0 \quad (35)$$

with the boundary conditions

$$w_1 = 0 \quad at \quad r_1 = \beta, \; and \quad r_2 = 1 + \epsilon\, cos(2\pi z). \quad (36)$$

By solving the above two systems using the Mathematica program, the analytic solution of w_0 and $w_1$will be found as follows:

$$w_0(r) = -\frac{1}{-e^{r_1/2} + e^{r_2/2}}e^{-r/2}(-e^{\frac{r}{2}+\frac{r_1}{2}} + e^{\frac{r}{2}+\frac{r_2}{2}} + 2\left(\frac{dp}{dz}\right)e^{\frac{r}{2}+\frac{r_1}{2}}r - 2\left(\frac{dp}{dz}\right)e^{\frac{r}{2}+\frac{r_2}{2}}r - 2\left(\frac{dp}{dz}\right)e^{\frac{r}{2}+\frac{r_1}{2}}r_1 + 2\left(\frac{dp}{dz}\right)e^{\frac{r_1}{2}+\frac{r_2}{2}}r_1 + 2\left(\frac{dp}{dz}\right)e^{\frac{r}{2}+\frac{r_2}{2}}r_2 - 2\left(\frac{dp}{dz}\right)e^{\frac{r_1}{2}+\frac{r_2}{2}}r_2)$$

$$w_1(r) = \frac{1}{12\left(e^{r_1/2} - e^{r_2/2}\right)^4}e^{-3r/2}(-12\left(\frac{dp}{dz}\right)^3 e^{r+2r_1+\frac{r_2}{2}}rr_1 + 36\left(\frac{dp}{dz}\right)^3 e^{r+\frac{3r_1}{2}+r_2}rr_1 - 36\left(\frac{dp}{dz}\right)^3 e^{r+r_1+\frac{3r_2}{2}}rr_1 + 12\left(\frac{dp}{dz}\right)^3 e^{r+\frac{r_1}{2}+2r_2}rr_1 + 12\left(\frac{dp}{dz}\right)^3 e^{r+2r_1+\frac{r_2}{2}}r_1{}^2 - 24\left(\frac{dp}{dz}\right)^3 e^{r+\frac{3r_1}{2}+r_2}r_1{}^2 - 12\left(\frac{dp}{dz}\right)^3 e^{\frac{r}{2}+2r_1+r_2}r_1{}^2 + 12\left(\frac{dp}{dz}\right)^3 e^{r+r_1+\frac{3r_2}{2}}r_1{}^2 + \cdots + 24\frac{dp}{dz}^3 e^{r+2r_1+\frac{r_2}{2}}r_2Log(r_2) + 48\left(\frac{dp}{dz}\right)^3 e^{\frac{3r}{2}+r_1+r_2}r_2Log(r_2) - 48\left(\frac{dp}{dz}\right)^3 e^{r+\frac{3r_1}{2}+r_2}r_2Log(r_2) - 24\left(\frac{dp}{dz}\right)^3 e^{\frac{3r}{2}+\frac{r_1}{2}+\frac{3r_2}{2}}r_2Log(r_2) + 24\left(\frac{dp}{dz}\right)^3 e^{r+r_1+\frac{3r_2}{2}}r_2Log(r_2))$$

4. Graphical Discussion

In this section, we will examine the physical impact of various flow interesting parameters on velocity profile, temperature distribution, concentration field, heat transfer coefficient, and stream function.

4.1. Velocity Profile

Figures 2-3 represent the velocity profile at different values of the physical parameters and variables. The plots elucidate that the behavior of the velocity profile is parabolic. Figures 2(a) and 2(b) are plotted to describe the effect of variation of pressure gradient $\frac{dp}{dz}$ and the Sutterby fluid parameter α on the velocity profile. The figures revealed that the fluid velocity reduces for enhanced values of $\frac{dp}{dz}$ and the parameter . The influence of the radius ratio β and amplitude ratio ϵ on velocity profile are plotted in Figures 3(a) and 3(b). It can be noticed that a rise in β and ϵ lead to an increment in velocity profile.

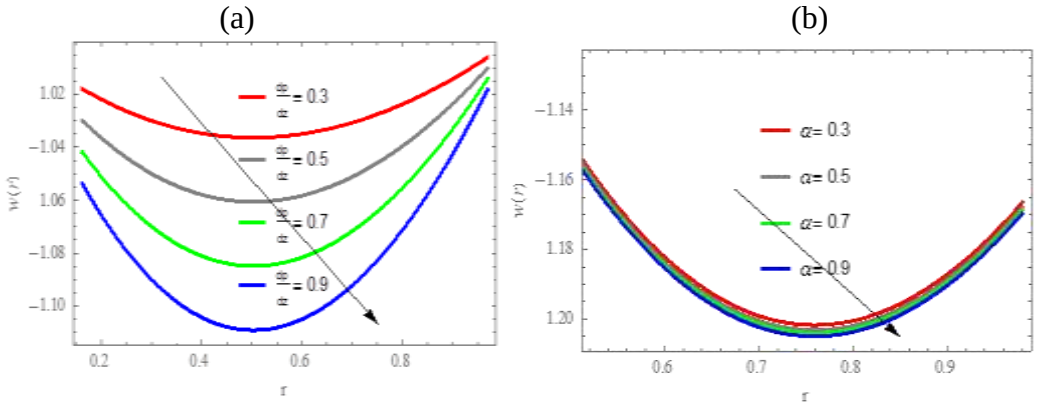

Figure2: Velocity curve for rising values of (a) gradient of pressure $\frac{dp}{dz}$ (b) Sutterby fluid parameter α and for fixed $\{\epsilon = 0.02, z = 0.1, \beta = 0.03\}$.

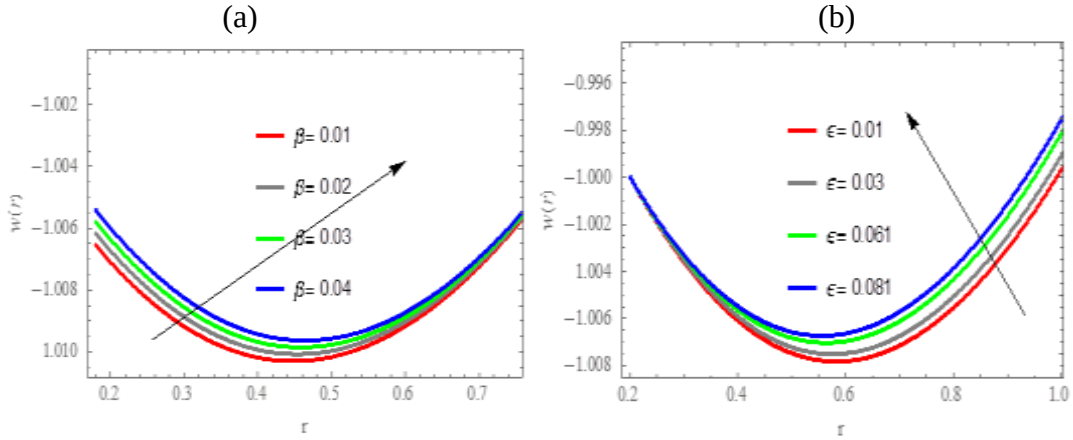

Figure 3: Velocity profile for different values of (a) endoscope radius ratio β (b) Amplitude ratio ϵ and fixed values of parameters$\{z = 0.1, \alpha = 0.03\}$.

4.2. Temperature Profile

Figures 4-6 display the behavior of the temperature profile for different magnitudes of the parameters $(\mathrm{Rn}, \beta, \epsilon, \mathrm{Du}, \mathrm{Pr}\ \text{and}\ \mathrm{Sc})$. It is clear from the plots that the temperature profile's attitude is a concave down as well as the maximum values can be seen in the middle region of the channel. Figures 4(a) and 4(b) recorded the graphical manner of temperature $\theta(r)$ against r, in these graphs the temperature $\theta(r)$ enhanced as radiation parameter Rn rises, whereas two opposite influences are seen via ascending value of tube radius ratio parameter β. The behaviors of the ratio amplitude parameter ϵ, and the Dufour parameter Du, on $\theta(r)$

are recorded in Figures 5(a), and 5(b). It is noticed that an increment value of ratio amplitude parameter ϵ tends $\theta(r)$ profile to increase on the left side of the figure for $(0 \leq r \leq 1.2)$ whereas the profile's behavior is reflected into diminishing on the right side for $(1.3 \leq r \leq 2.5)$, however, a reduction effect of Du on temperature profile along the channel length while a little increment in the central part of the channel is seen. Similar influence for Prandtl number Pr and the Schmidt number Sc on temperature profile is indicated in Figures 6(a), and 6(b).

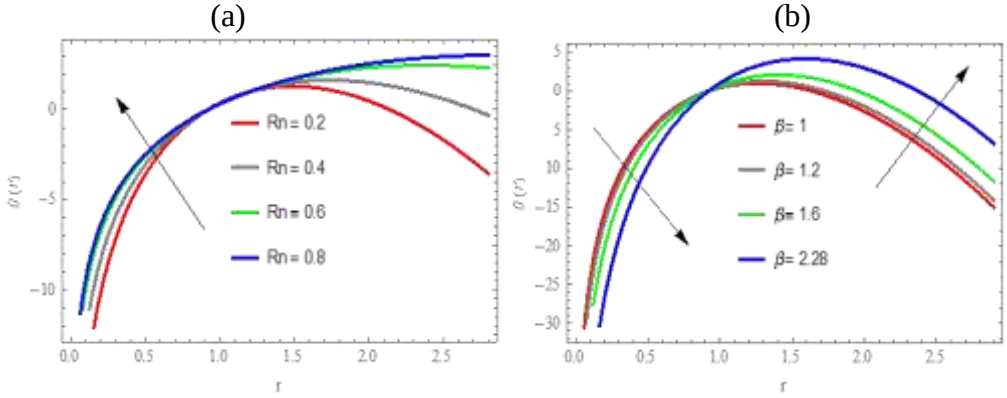

Figure 4: Temperature distribution for ascending in (a) Radiation parameter Rn, (b) radius ratio parameterβ, with the for fixed values of parameters$\{B = 2.85, \epsilon = 0.1, z = 0.6, \beta = 1.2, Du = 0.8, Pr = 1.2, Sc = 1.1, Sr = 1.5\}$.

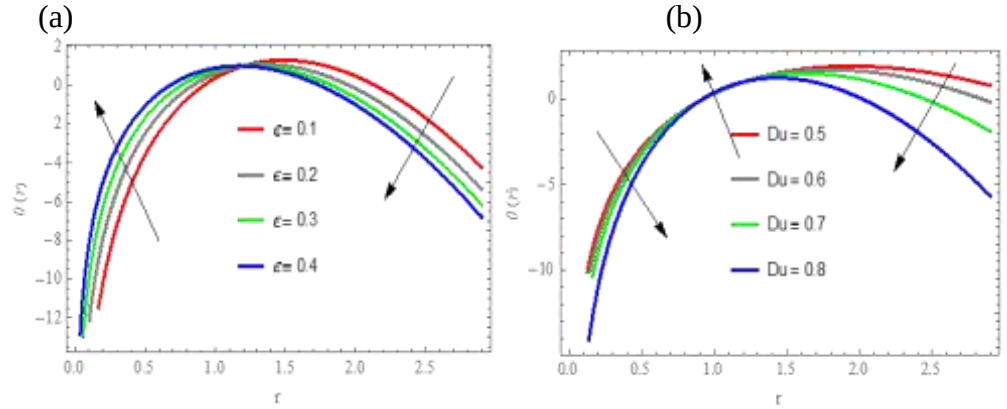

Figure 5: Temperature distribution for ascending of (a) Amplitude ratio ϵ (b) Dufour number Du , and fixed $\{B = 2.85, Rn = 1, z = 0.6, \beta = 1.2, Pr = 1.2, Sc = 1.1, Sr = 1.5\}$.

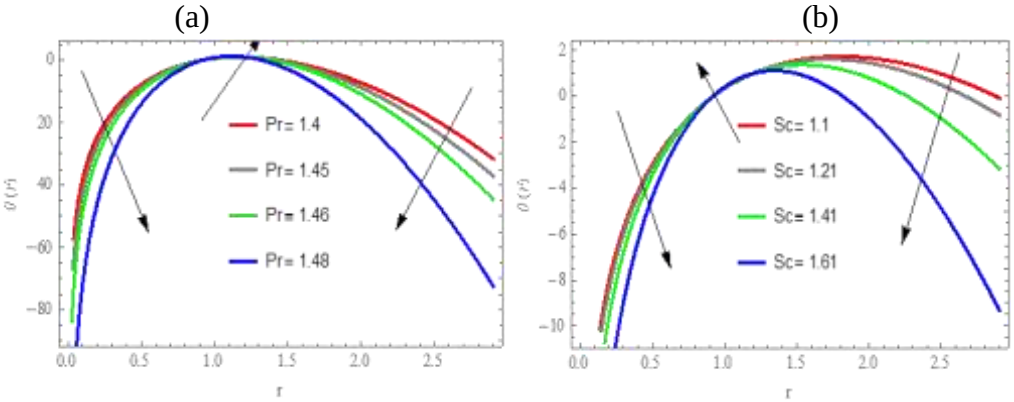

Figure 6: Temperature distribution for ascending of (a) Prandtl number Pr (b) Schmidt number Sc, and fixed $\{B = 2.85, \mathrm{Rn} = 1, z = 0.6, \beta = 1.2, \mathrm{Du} = 0.8, \mathrm{Pr} = 1.2{,}1.1, \mathrm{Sr} = 1.5\}$.

4.3. Concentration profile

The variation in concentration profile with the ascending values of the interesting physical parameters within its function is discussed in this subsection through Figures 7- 9. It is apparent from these plots that the maximum values for fluid concentration appear in the central part arising in a parabolic trajectory. Figures 7(a), 7(b), and 8(a) are plotted to report the impact of the parameters $(\mathrm{Du}, \mathrm{Pr}, and\ Sc)$ on concentration profile $\eta(r)$. An increase in Du, Pr, and Sc cause concentration to increase as we move further toward the boundaries whereas a decrease in $\eta(r)$ profile is noticed further from the walls i.e. near the central. The concentration profile exhibit two opposite behavior via growing β magnitude see Figure 8(b). It is identified in Figure 9(a) that on increasing the value of Rn, the concentration profile declines near the boundaries while little arises is seen near the central part of the channel. Figure 9(b) demonstrates an increase in $\eta(r)$ profile with a higher magnitude of non-dimensional heat source parameter B.

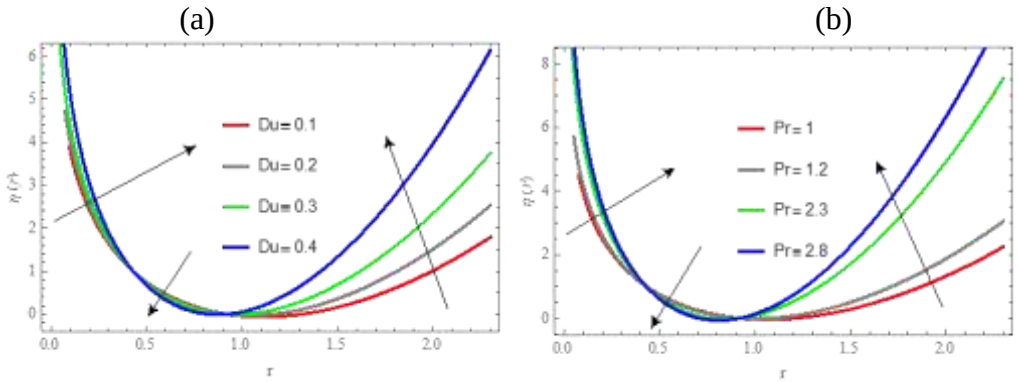

Figure 7: Concentration distribution with rise values of (a) Dufour number Du (b) Prandtle number Pr, for fixed values of parameters $\{B = 2.85, \mathrm{Rn} = 1, z = 0.6, \beta = 1.2, \mathrm{Du} = 0.8, \mathrm{Sc} = 1.2{,}1.1, \mathrm{Sr} = 1.5\}$.

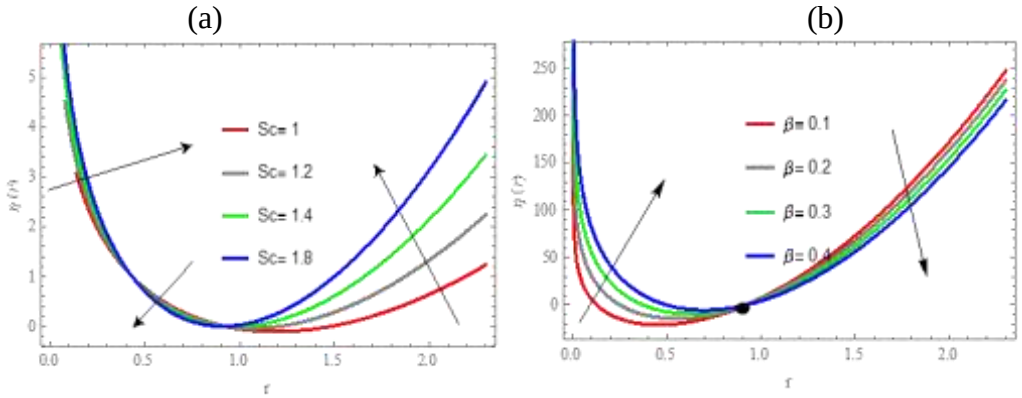

Figure 8: $\eta(r)$ for ascending (a) Schmidt number Sc (b) radius ratio parameterβ and for fixed values of parameters $\{B = 2.85, \mathrm{Rn} = 1, z = 0.6, \epsilon = 0.2, \mathrm{Du} = 0.8, \mathrm{Sc} = 1.2{,}1.1, \mathrm{Sr} = 1.5\}$.

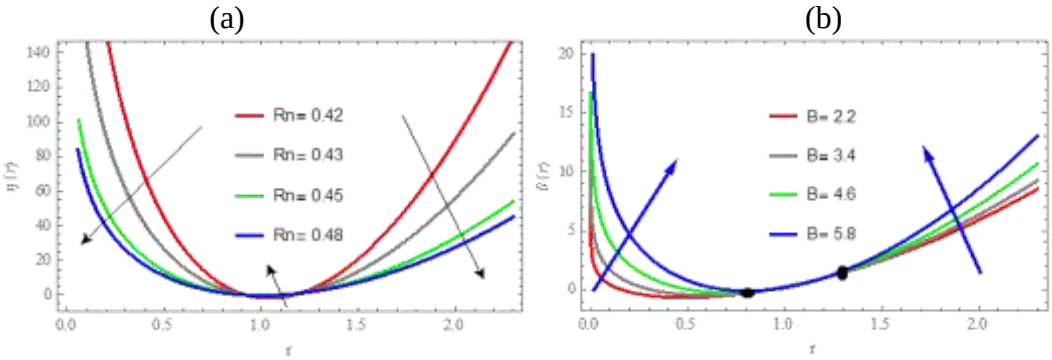

Figure 9: concentration profile $\eta(r)$ for different values of (a) thermal radiative number Rn (b) heat source parameter$B$ and for fixed values of parameters $\{pr = 1, \beta = 1, z = 0.6, \epsilon = 0.2, \mathrm{Du} = 0.8, \mathrm{Sc} = 1.2{,}1.1, \mathrm{Sr} = 1.5\}$.

4.4. Heat Transfer

Figures 10(a-d) elucidate the impact of the Dufour number Du, Soret number Sr, Prandtl number Pr, and radiation parameter Rn on the coefficient of heat transfer at the lower wall profile against the transverse axial z. These figures show an oscillatory behavior of *H (z)* via the flow of peristaltic waves along the channel wall. Figure 10(a) portrays the increasing function of the heat transfer coefficient due to arise in Rn value. However, Figures 10(b)-(d) show that the heat transfer rate reduced for ascending magnitude of Du, Sr, and Pr.

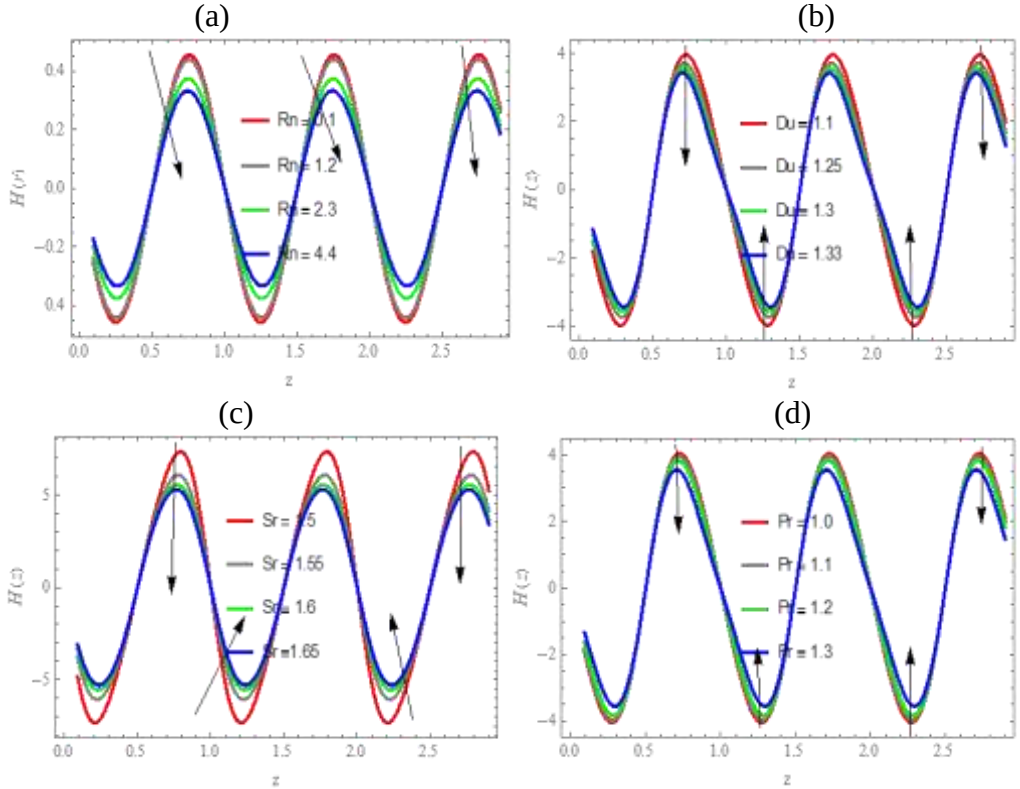

Figure 10: Heat transfer coefficient *H (z)* for different values of (a) Radiation parameter Rn (b) Dufour number Du (c) Soret parameter Sr (d) Prandtl number Pr and fixed parameter $\{B = 3.08, , \epsilon = 0.1, r = 0.4, \beta = 0.3, \mathrm{Sc} = 1.91, \}$.

4.5. Trapping phenomenon

An attractive phenomenon in peristaltic motion is trapping, where the streamlines will split to trap a bolus of fluid moving along the channel walls. We take the absolute value of the stream function to solve the equation of ψ. Figures 11-14 highlight the impact of Pressure

gradient $\frac{dp}{dz}$, Sutterby fluid parameter α , ratio amplitude parameter ϵ, and radius ratio parameter β on the trapping bolus. Figure 11 depicts the variation of $\frac{dp}{dz}$ magnitude on the trapping bolus. It is evident that with a rise in $\frac{dp}{dz}$, the numbers and volume of the bolus are enhanced. The action of Sutterby fluid parameter α on the trapped bolus is recorded in Figure12. The magnitude of the trapping bolus diminished in size and more bolus and streamlines were created. The effect of ratio amplitude parameter ϵ is increasing effect on the trapped bolus see Figure 13. However, Figure14 recorded the decreasing impact of radius ratio parameter β on the trapping phenomenon.

(a) (b)

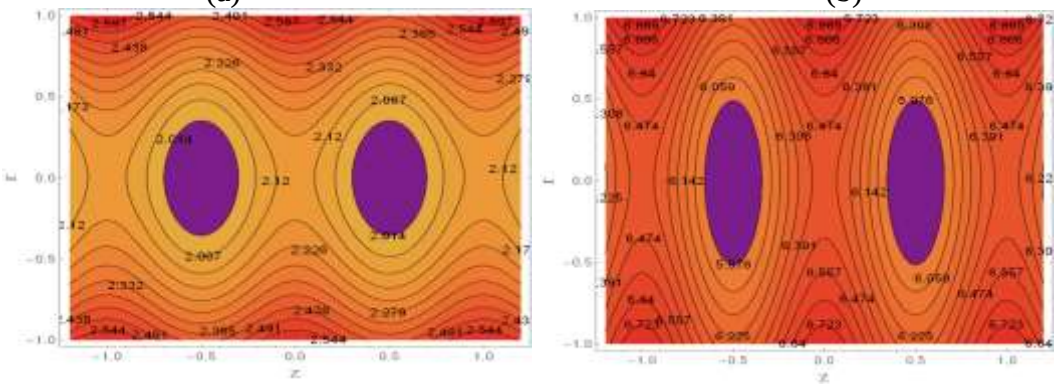

Figure 11: Streamlines for variation of the gradient of Pressure $\frac{dp}{dz} = \{0.1, 0.8\}$with $\{\alpha = 0.01, \epsilon = 0.2, \beta = 0.02\}$.

(a) (b)

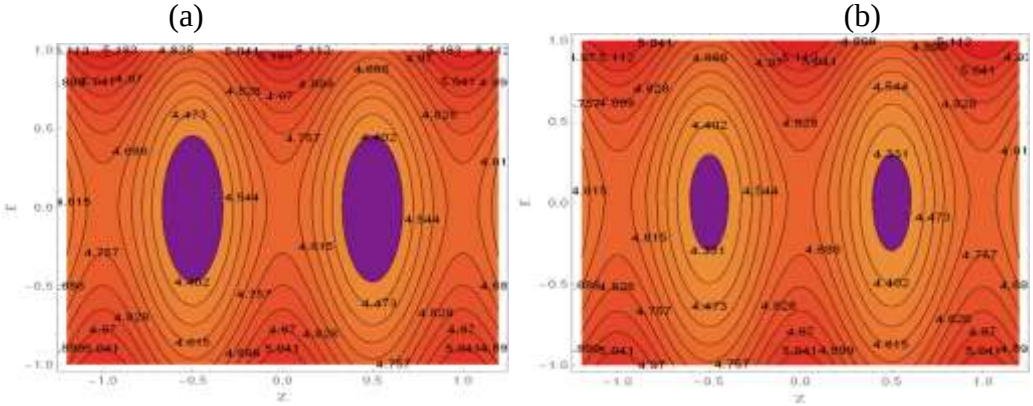

Figure 12: Streamlines for variation of Sutterby fluid parameter $\alpha = \{0.2,0.4\}$ with $\{\epsilon = 0.2, \beta = 0.2\}$.

(a) (b)

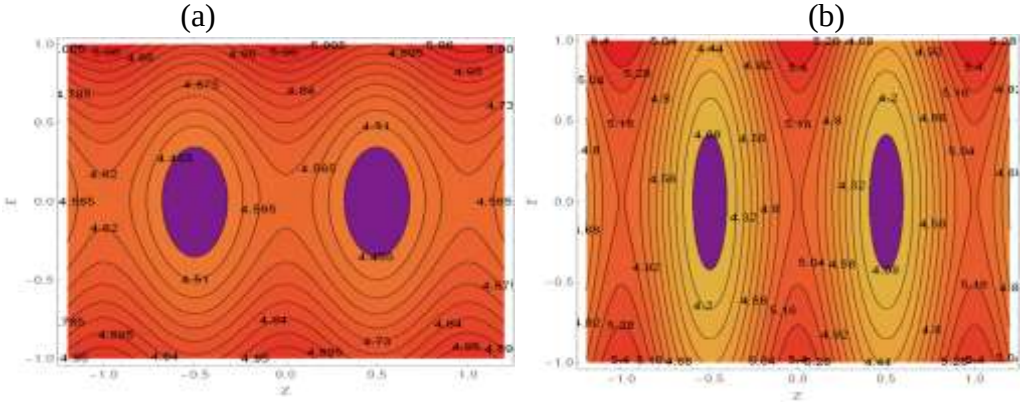

Figure 13: Streamlines for variation of Sutterby fluid parameter $\epsilon = \{0.3, 0.6\}$ with $\{\alpha = 0.1, = 0.2\}$.

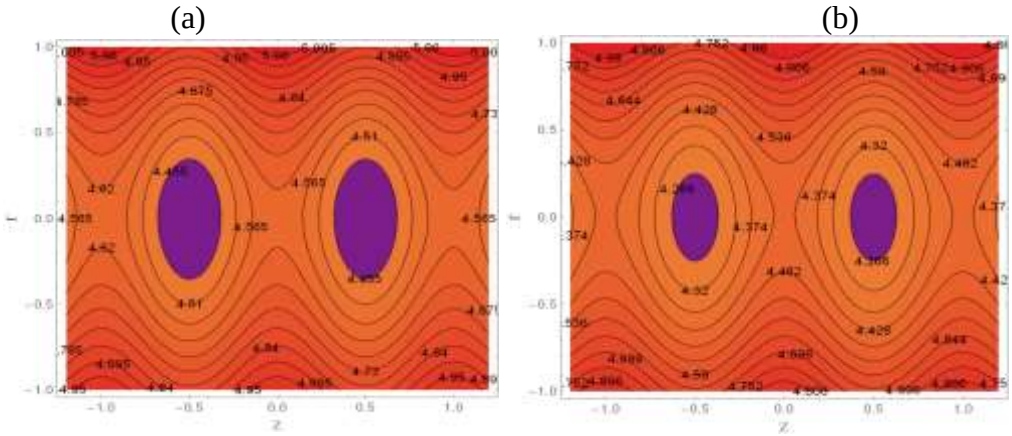

Figure 14: Streamlines for variation of radius ratio parameter $\beta = \{0.2, 0.6\}$ with $\{\alpha = 0.1, \epsilon = 0.1\}$.

5. Conclusions

In this paper, a new mathematical formulation is presented to analyze the effect of endoscope on the peristaltic transport of non-Newtonian Sutterby fluid through a tube. The exact solution for the temperature and concentration field is found, while the perturbation scheme is employed for the analytic solution of the velocity field. The study came out with major conclusions that are listed as follows:

1. The velocity profile is parabolic along with the whole range of the r-axis for various values of the $\frac{dp}{dz}$, the Sutterby fluid parameter α, the endoscope radius ratio β, and amplitude ratio parameter ϵ in the peristaltic flow of Sutterby fluid in tubes. Moreover, the minimum values of the velocity were recognized near the endoscope tube.
2. The magnitude of the velocity profile increases with increasing β, and ϵ, whereas it decreases with increasing $\frac{dp}{dz}$, and α .
3. The temperature distribution against $r-$ axis shows a concave down behavior along the length of tubes, on the contrary, the concentration profile has a concave up nature through the region between the tubes.
4. An improvement in temperature is yielded out with enhancing Rn parameter in comparison with the concentration profile.
5. An oscillatory behaviour for temperature profile is observed due to β and ϵ increment values.
6. We noticed retardation in $\theta(r)$ toward the boundaries but the reverse effect is noticed near the central part of the tube for Du, Pr, and Sc , this analysis is reversed for the concentration profile.
7. The heat transfer coefficient at the outer wall has an oscillatory profile because of the propagation of the sinusoidal waves travelling along the wall of the tube with the rise of $Rn, Du, Sr,$ and Pr.
8. The number and the size of the trapped bolus are growing with the increase of $\frac{dp}{dz}$, and ϵ, respectively, while the trapped bolus is contracting and decreasing with increasing in α, and β.
9. The results calculated within the research are commensurate with others calculated in the references [1,23]. Furthermore, the Sutterby model fluid is one of the most important non-Newtonian fluids which represents constitutive equations for high polymer aqueous solutions of CMC, HEC, and MC. Hence, the problem is of practical significance in modern industrial and scientific aspects.

References

[1] A. T. V. Kotnurkar A.S., " “Influence of Jeffrey Nanofluid on Peristaltic Motion in an Inclined Endoscope”," *Computational Engineering and Physical Modeling,* vol. 4, pp. 68-94, 2021.

[2] T. W. Latham, "Fluid motions in a peristaltic pump.", PhD diss., Massachusetts Institute of Technology, 1966.

[3] J. M. a. W. S. Shapiro A.H., " “Peristaltic pumping with long wavelengths at low Reynolds number”," *Fluid. Mech,* vol. 37, pp. 799-825, 1969.

[4] a. S. A. H. Jaffrin M.Y., " “Peristaltic pumping”," *Annu. Rev. Fluid,* vol. 3, pp. 13-36, 1971.

[5] T. M. R. a. B. A. Hayat, "Hayat, Tasawar, Maimona Raf "Soret and Dufour effects on MHD peristaltic flow of Jeffrey fluid in a rotating system with porous medium."," *PloS one Journal,* vol. 11, p. e0145525, 2016.

[6] a. S. G. Asha SK., " “Effect of couple stress in peristaltic transport of blood flow by homotopy analysis method”," *Asian Journal of Science and Technology,* vol. 12, pp. 6958-64, 2017.

[7] a. S. G. Asha SK., "Ash “Mixed convection peristaltic flow of an Eyring–Powell nanofluid with magnetic field in a non-uniform channel”," *Asha SK., and Sunitha G., “Mixed convection peristaltic flow of an Eyring–Powell naJournal of Applied Mathematics and Computation,* vol. 2, p. 332–4, 2018.

[8] a. S. G. Asha SK., "“Peristaltic transport of Eyring-Powell nanofluid in a non-uniform channel”," *Jordan J. Math. Stat.,* vol. 12, p. 431–53, 2019.

[9] L. J. Fauci, "“Peristaltic pumping of solid particles”," *Computers Fluids,* vol. 21, pp. 583-598, 1992.

[10] a. H. T. Brown T. D., " “Computational and experimental investigations of two-dimensional nonlinear peristaltic flows”," *Journal of Fluid Mechanics,* vol. 83, p. 249–272, 1977.

[11] S. V. P. a. S. S. N. Srivastava L. M., "Srivastava L. M., Srivastav “Peristaltic transport of a physiological fluid Part I. Flow in non-uniform geometry”," *Biorheology,* vol. 20, p. 153–166, 1983.

[12] a. S. V. P. Srivastava L. M., "Srivastava L. M. “Peristaltic transport of a power-law fluid: application to the ductus afferents of the reproductive tract”," *Rheologica Acta,* vol. 27, p. 428–433, 1988.

[13] E. A., "“A new numerical solution for the MHD peristaltic flow of a bio-fluid with variable viscosity in a circular cylindrical tube via Adomian decomposition method”," *Physics Letters A,* vol. 372, pp. 5321-5328, 2008.

[14] A. a. S. M. K. Ebaid, ""An exact solution for a boundary value problem with application in fluid mechanics and comparison with the regular perturbation solution."," *Abstract and Applied Analysis,* vol. 2014, 2014.

[15] M. R. S. a. H. A. Ali, " “Approximate Treatment for The MHD Peristaltic Transport of Jeffrey Fluid in Inclined Tapered Asymmetric Channel with Effects of Heat Transfer and Porous Medium”," *Iraqi Journal of Science,* vol. 61, pp. 3342-3354, 2020.

[16] D. R. Raju KK, "“Peristaltic Motion of a non-Newtonian fluid”," *Rheol Acta,* vol. 11, pp. 170-8, 1972.

[17] H. Z. M. M. a. A. A. Hayat T., " “Peristaltic flow of Sutterby fluid in a vertical channel with radiative heat transfer and compliant walls: A numerical study”," *Results in Physics journal,* vol. 6, pp. 805-810, 2016.

[18] S. Q. T. H. a. A. A. Muhammad Ijaz Khan, "Muhammad Ijaz Khan, Sumaira Qayyum, Tasawa “Stratified flow of Sutterby fluid with homogeneous-heterogeneous reactions and Cattaneo-Christov heat flux”," *Nonlinear Analysis and Applied Mathematics (NAAM) Research Group,* vol. 2977, 2019.

[19] F. M. S. Q. a. A. A. Tasawar Hayat, " “Sutterby fluid flow subject to homogeneous-heterogeneous reactions and nonlinear radiation”," *Journal Pre-proof,* 2016.

[20] K. G. a. S. B. P. R. Venkata M. Subba Rao, " “Sutterby fluid flow past a stretching sheet

embedded in a porous media with viscous dissipation”," *International Journal of Ambient Energy,* 2021.

[21] M. J. M. B. R. A. a. S. S. Mabood F., " “Dynamics of Sutterby fluid flow due to a spinning stretching disk with non-Fourier/Fick heat and mass flux models”," *App. Math. Mech.,* 2021.

[22] A. S. A. A. T. A. a. A. B. Hayat T., " “Numerical simulation for the peristaltic activity of Sutterby fluid with modified Darcy’s law”," *Results in Physics journal,* vol. 7, pp. 762-768, 2017.

[23] a. D. M. Ramesh K., "“Effect of endoscope on the peristaltic transport of a couple of stress fluid with heat transfer, Application to biomedicine”," *Nonlinear Eng. ,* vol. 8, pp. 619-29, 2019.

[24] S. A. T. A. a. A. F. Hayat T., "“Numerical study for MHD peristaltic flow of Williamson nanofluid in an endoscope with partial slip and wall properties”," *Int. J. Heat Mass Transf.,* vol. 114, pp. 1181-7, 2017.

[25] H. A. Ali, " “Radiative peristaltic transport of Ree-Eyring fluid through a porous medium in asymmetric channel subjected to the combined effect of inclined MHD and convective conditions”," *Journal of Physics: Conference Series,* 2021.